

# All-sky Galactic radiation at 45 MHz and spectral index between 45 and 408 MHz

A. E. Guzmán<sup>1</sup>, J. May<sup>1</sup>, H. Alvarez<sup>1</sup>, and K. Maeda<sup>2</sup>

<sup>1</sup> Departamento de Astronomía, Universidad de Chile, Casilla 36-D, Santiago, Chile

<sup>2</sup> Hyogo University of Health Sciences

Received / Accepted

## ABSTRACT

**Aims.** We study the Galactic large-scale synchrotron emission by generating a reliable all-sky spectral index map and temperature map at 45 MHz.

**Methods.** We use our observations, the published all-sky map at 408 MHz, and a bibliographical compilation to produce a map corrected for zero-level offset and extragalactic contribution.

**Results.** We present full sky maps of the Galactic emission at 45 MHz and the Galactic spectral index between 45 and 408 MHz with an angular resolution of  $5^\circ$ . The spectral index varies between 2.1 and 2.7, reaching values below 2.5 at low latitude because of thermal free-free absorption and its maximum in the zone next to the Northern Spur.

**Key words.** Surveys - Galaxy: general - Radiation mechanisms: non-thermal - Radio continuum: ISM

## 1. Introduction

A way to describe some global features of our Galaxy is to perform radio observations that span large areas of the sky. Below 1.4 GHz, there are few surveys with large coverage and all-sky maps such as the 408 MHz maps of Haslam et al. (1981, 1982) and the 1420 MHz maps of Reich (1982), Reich & Reich (1986), and Reich et al. (2001). The 45 MHz survey presented in this paper covers 96% of the sky.

This frequency range probes mostly the synchrotron emission from high energy electrons interacting with the large-scale magnetic field of the Galaxy and the spectral information derived at these frequencies is related to the spectral energy distribution of these relativistic electrons. Spectral index maps are presented in Reich et al. (2004) between the frequencies 408, 1420, and 22800 MHz. The subject has also received attention in its application to the problem of adequately subtracting the foreground radiation from the cosmic microwave background (de Oliveira-Costa et al. 2008).

Important physical information can be extracted from the surveys and the spectral index maps concerning Galactic structure, global magnetic fields and relativistic electron distribution. In this paper, we present an all-sky spectral index map by using our 45 MHz survey and the 408 MHz (Haslam et al. 1981, 1982) all-sky map, together with multi-frequency studies of six zones that allow us to obtain zero-level corrections for both maps. In the Appendix, we estimate the extragalactic background non-thermal spectrum based on a literature compilation.

## 2. The 45 MHz survey

The 45 MHz southern and northern sky maps (Alvarez et al. 1997b, Maeda et al. 1999) were com-

bined in the all-sky map<sup>1</sup> shown in Fig. 1. Missing data around the north equatorial pole represents  $\sim 4\%$  of the whole sky. The southern map data were observed between 1982 and 1994 with an array of 528 E-W dipoles that produced an effective beam of  $4.6^\circ(\alpha) \times 2.4^\circ(\delta)$  FWHM. A full description of the instrument was given by May et al. (1984) and an experimental determination of the beam in Alvarez et al. (1994). The northern data were taken in the periods of 1985-1989 and 1997-1999 with the MU radar array (Fukao et al. 1985a,b) at an angular resolution of  $3.6^\circ \times 3.6^\circ$ . Table 1 displays some of the principal characteristics of southern and northern parts of the 45 MHz survey.

An important characteristic of the all-sky 45 MHz map is that it consists of only two surveys and uses only two transit instruments with similar characteristics. Some relevant features of this map are:

1. Galactic plane: Most of the emission at 45 MHz comes from the plane of the Galaxy that has an overall maximum near the Galactic center. Figure 2 shows the plane profiles averaged inside the  $|b| < 10^\circ$  strip for the 45 and 408 MHz surveys, both convolved to the common  $5^\circ \times 5^\circ$  resolution. We can see that most of the structure of the 408 MHz Galactic plane is reproduced in the 45 MHz plane. This structure includes the strong maximum near the Galactic center (note that the 45 MHz map reaches its maximum at approximately  $l = 2^\circ$ , as discussed in Alvarez et al. 1997a), the “steps” in the emission produced by the spiral arms can be seen tangentially, and some strong sources exist near the plane. The 45 MHz map shows more conspicuously sources associated with non-thermal emission (such as the Galactic center and

<sup>1</sup> The 45 MHz map can be downloaded from the website <http://www.das.uchile.cl/survey45mhz>.

Table 1: Parameters of the Northern and Southern surveys.

Array	Coverage	Effective Area	Operating frequency	Resolution (FWHM)
Maipú	$-90^\circ \leq \delta \leq +19.1^\circ$	11200 m <sup>2</sup>	45 MHz	$4.6^\circ(\alpha) \times 2.4^\circ(\delta)$
MUradar	$+5^\circ \leq \delta \leq +65^\circ$	8300 m <sup>2</sup>	46.5 MHz	$3.6^\circ \times 3.6^\circ$

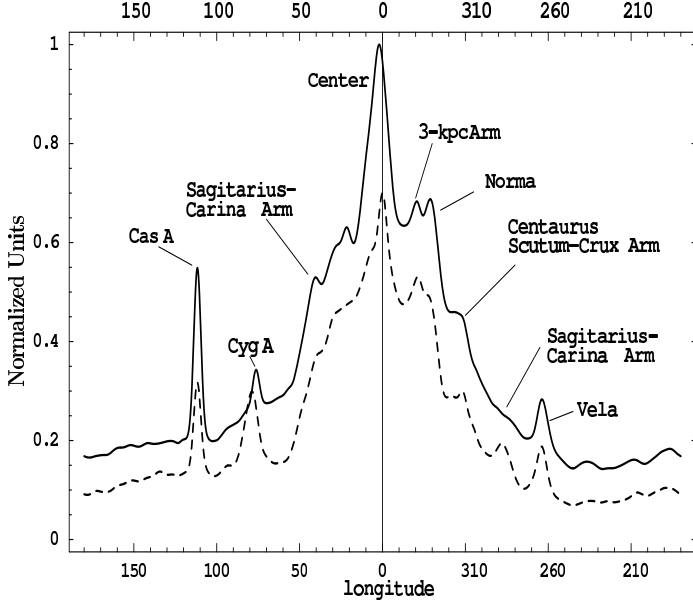


Fig. 2: Temperature averaged across longitude in the  $|b| < 10^\circ$  strip from 45 MHz (continuous) and 408 MHz (dashed) surveys in arbitrarily normalized units:  $T(45 \text{ MHz})/(54000 \text{ K})$  and  $T(408 \text{ MHz})/(300 \text{ K})$ . The "steps" mark the tangential directions to spiral arms.

Cas A), compared to the 408 MHz map that shows strong thermal sources as well.

- Northern spur: This feature forms an arc from  $l \approx 35^\circ$ ,  $b \approx 16^\circ$  passing through  $l \approx 0^\circ$ ,  $b \approx 75^\circ$  and ending near the position of Virgo A. The hypothesis that this is a nearby supernova remnant shell is an old one (Hanbury Brown et al. 1960) and has become widely accepted (see Wolleben 2007 and references therein).
- Galactic and extragalactic sources: i) Galactic: SNR Cas A ( $l = 111.5^\circ$ ,  $b = -2.3^\circ$ ), Vela SNR ( $l = 263.9^\circ$ ,  $b = -3.3^\circ$ ), and the direction of the Local arm towards Cygnus and Vela. ii) Extragalactic: Radio-galaxies such as Cen A ( $l = 309.5^\circ$ ,  $b = 19.4^\circ$ ), Cyg A ( $l = 76.2^\circ$ ,  $b = 5.8^\circ$ ), Virgo A ( $l = 285^\circ$ ,  $b = 74.3^\circ$ ), Hydra A ( $l = 243^\circ$ ,  $b = +25^\circ$ ), Pictor A ( $l = 252^\circ$ ,  $b = -34^\circ$ ), and Fornax A ( $l = 240^\circ$ ,  $b = -56.3^\circ$ ). We can also distinguish the Large Magellanic Cloud at  $l = 280.2^\circ$ ,  $b = -32.8^\circ$ .
- Minimum temperature zones: There are two areas with minima of temperature, one in the southern Galaxy ( $l \sim 235^\circ$ ,  $b \sim -45^\circ$ ,  $T \sim 3600 \text{ K}$ ) and the other in the north ( $l \sim 192^\circ$ ,  $b \sim 48^\circ$ ,  $T \sim 3800 \text{ K}$ ). It is remarkable that these two points are rather close in Galactic longitude, at approximately the point where the Galactic plane reaches its minimum temperature compared to other longitudes ( $T \sim 8000 \text{ K}$ ,  $l \sim 225^\circ$ , see Fig. 2). It is in these directions that any extragalactic or instrumental

feature should be most noticeable. These two zones are later discussed in detail.

### 3. Spectral index map

From observations at two frequencies  $\nu_1$  and  $\nu_2$ , we can derive the "temperature spectral index"  $\beta_{\nu_1-\nu_2}$  between these frequencies, defined as

$$\beta_{\nu_1-\nu_2} = -\log\left(\frac{T_{\nu_1}}{T_{\nu_2}}\right) / \log\frac{\nu_1}{\nu_2}, \quad (1)$$

where  $T_{\nu_1}$  and  $T_{\nu_2}$  are the respective brightness temperatures.

At 45 and 408 MHz, the relation between the brightness temperature and the intensity of the radiation approximately follows the Rayleigh-Jeans law, which implies that it is a simple relation between the temperature spectral index  $\beta$  and the intensity spectral index  $\alpha$  given by  $\beta = \alpha + 2$ .

To calculate these spectral indices appropriately it is necessary to use brightness temperatures measured at the same resolution. Because of the difference in beam-size (and shape) between the surveys at 45 and 408 MHz, we convolved each map to  $5^\circ$  FWHM.

The measured temperature  $T_\nu$  at frequency  $\nu$  is modeled as

$$T_\nu = T_{\nu,G} + T_{\nu,0} = T_{\nu,G} + T_{CMB} + T_{\nu,Ex} + T_{\nu,ZLC} \quad (2)$$

with a Galactic component  $T_{\nu,G}$  and an isotropic one  $T_{\nu,0}$  (the "offset"), which includes the non-thermal extragalactic background ( $T_{Ex}$ ), the CMB ( $T_{CMB}$ ), and a zero-level correction ( $T_{ZLC}$ ). To obtain a spectral index associated with Galactic emission, we need to correct the observed temperature by subtracting the offset temperature. If the spectral index  $\beta$  due to Galactic emission is constant in some area, then the following relations hold:

$$T_{\nu,G} = (T_\nu - T_{\nu,0}) \propto \nu^{-\beta},$$

$$\frac{T_{\nu_1} - T_{\nu_1,0}}{T_{\nu_2} - T_{\nu_2,0}} = \left(\frac{\nu_1}{\nu_2}\right)^{-\beta}. \quad (3)$$

#### 3.1. Zero-level correction of the 45 and 408 MHz surveys

On the basis of published data at different frequencies, we constructed a multi-frequency spectrum at selected and well-observed positions of the sky. We use these spectra to determine the zero-level correction temperature for the 45 and 408 MHz surveys. This zero level is a second order correction to the already calibrated data, and the method presented here is an alternative to the more common approach of using TT-plots (see e.g. Reich & Reich 1988a). The six selected positions are:

- The Galactic poles and the anticenter: these regions were chosen because we expect a minimal amount of Galactic thermal absorption in these directions.

Table 2: Multifrequency data for the selected points. The asterisks indicate data not included in the multifrequency fit.

$\nu$ [MHz]	Anti. [K]	Calib. Point [K]	Minim. North [K]	Minim. South [K]	NGP [K]	SGP [K]	Ref.
1.6	...	...	...	* 6.5E6 ± 5.E5	...	...	1
2.3	...	...	...	...	1.1E7 ± 1.E6	1.8E7 ± 1.E6	2
4.7	...	...	...	* 1.88E6 ± 4.E5	...	...	3
4.7	...	...	...	* 1.38E6 ± 1.E5	...	...	4
5.2	...	...	...	...	1.7E6 ± 4.E5	1.3E6 ± 3.E5	5
5.5	...	...	...	* 7.5E5 ± 2.E5	...	...	4
8.3	...	...	...	* 5.E5 ± 1.E5	...	...	4
9	...	...	...	...	4.E5 ± 6.E4	4.2E5 ± 6.E4	5
10	2.9E5 ± 1.E4	...	1.3E5 ± 1.E4	...	...	...	6
10.02	...	...	...	* 6.E5 ± 1.E5	...	7.E5 ± 3.E5	7
13	...	...	...	* 1.25E5 ± 3.E4	...	...	4
13.1	2.5E5 ± 5.E3	...	...	...	...	...	8
13.1	...	...	8.E4 ± 2.E4	...	...	...	9
13.5	...	...	...	...	1.17E5 ± 1.E4	...	10
14.1	...	...	...	* 1.1E5 ± 8.E3	...	1.25E5 ± 9.E3	11
15.6	...	...	...	...	9.9E4 ± 1.E4	9.8E4 ± 1.E4	5
16.5	...	...	...	* 1.E5 ± 2.E4	...	...	4
17.5	...	...	...	...	6.6E4 ± 6.E3	...	10
18.3	...	...	3.75E4 ± 1.E4	...	...	...	12
18.3	...	...	...	* 6.E4 ± 8.E3	...	7.5E4 ± 8.E3	12
20	...	...	...	...	...	5.53E4 ± 4.E3	11
22	4.45E4 ± 4.E3	1.4E5 ± 1.E4	...	...	...	...	14
23	...	...	...	...	3.1E4 ± 5.E3	3.E4 ± 5.E3	5
26	...	...	...	...	1.8E4 ± 1.E3	...	15
30	...	...	...	* 1.48E4 ± 1.E3	...	1.53E4 ± 9.E2	16
30	...	...	...	...	...	1.78E4 ± 1.E3	11
34.5	2.29E4 ± 1.E3	...	7.9E3 ± 7.E2	...	...	...	17
38	1.3E4 ± 1.E3	* 1.25E4 ± 1.E3	5.E3 ± 1.E3	...	...	...	18
38	...	...	...	...	...	...	19
38	1.32E4 ± 4.E2	3.45E4 ± 5.E2	...	...	...	...	20
38	...	...	...	...	9.E3 ± 1.E3	...	15
45	9.14E3 ± 9.E2	3.09E4 ± 3.E3	3.31E3 ± 3.E2	3.64E3 ± 4.E2	5.16E3 ± 5.E2	5.58E3 ± 6.E2	48
48.5	...	...	...	...	...	5.05E3 ± 4.E2	11
55	...	1.5E4 ± 1.E3	...	3.E3 ± 1.E3	...	...	21
81	1.8E3 ± 1.E2	...	5.E2 ± 1.E2	...	1.4E3 ± 5.E1	...	22
81.5	...	...	...	...	1120.	...	15
85	...	6.E3 ± 5.E2	...	...	...	...	23
85	...	...	...	...	...	1.2E3 ± 8.E1	11
85	...	...	...	9.5E2 ± 5.E1	...	1.35E3 ± 5.E1	24
85.7	...	...	...	...	...	...	25
100	1.13E3 ± 1.E2	...	5.25E2 ± 3.E1	4.4E2 ± 1.E2	7.E2 ± 5.E1	6.5E2 ± 5.E1	26
100	1.E3 ± 3.E2	...	...	...	...	...	27
102.5	...	5.5E3 ± 5.E2	...	...	...	...	28
150	...	2.25E3 ± 3.E2	...	...	...	...	29
150	...	1.8E3 ± 2E2	...	...	...	...	23
153	...	1.8E3 ± 2.E2	...	1.8E2 ± 2.E1	...	2.8E2 ± 2.E1	30
178	...	...	...	...	1.7E2 ± 1.E1	...	15
178	3.3E2 ± 1.E1	1.7E3 ± 5.E1	7.E1 ± 1.E1	...	1.4E2 ± 1.E1	...	31
200	...	...	...	1.04E2 ± 8.	...	...	32
200	2.4E2 ± 1.E1	...	1.35E2 ± 10.	...	...	...	33
200	1.42E2 ± 4.E1	...	...	...	...	...	27
250	1.4E2 ± 2.E1	...	...	...	1.04E2 ± 6.	1.07E2 ± 6.	34
320	6.E1 ± 5.	...	...	...	...	...	35
400	4.32E1 ± 2.	2.24E2 ± 3.E1	...	...	2.1E1 ± 1.	...	36
404	3.6E1 ± 1.	...	1.65E1 ± 5.E-1	...	2.E1 ± 1.	...	37
408	4.3E1 ± 1.	...	...	...	...	...	38
408	...	1.08E2 ± 2.E1	...	...	...	...	39
408	...	...	...	...	...	1.95E1 ± 2.	40
600	...	8.E1 ± 5.	...	...	...	...	41
610	...	...	6.6 ± 1.E-1	...	...	...	42
610	...	9.E1 ± 1.E1	...	...	...	...	43
820	8.5 ± 5.E-1	4.2E1 ± 6.	5. ± 5.E-1	...	...	...	44
1420	3.95 ± 5.E-2	...	...	...	3.4 ± 1.E-1	...	45
1420	...	1.05E1 ± 5.E-1	3.3 ± 1.E-1	...	...	...	46
1420	...	...	...	3.5 ± 5.E-2	...	3.6 ± 5.E-2	47

**Notes.** Columns names correspond to the positions described in Table 3.

**References.** (1) Ellis & Mendillo (1987); (2) Hartz (1964) ; (3) Ellis & Hamilton (1966); (4) Ellis (1982); (5) Cane (1979); (6) Caswell (1976); (7) Hamilton & Haynes (1968); (8) Andrew (1966); (9) Andrews (1969); (10) Bridle (1967);(11) Yates & Wielebinski (1965) (12); Shain (1951); (13) Shain & Higgins (1954); (14) Roger et al. (1999); (15) Purton (1966); (16) Mathewson et al. (1965); (17) Dwarakanath & Udaya Shankar (1990); (18) Blythe (1957); (19) Hornby & Williams (1966); (20) Milogradov-Turin & Smith (1973); (21) Rohan & Soden (1970); (22) Baldwin (1955); (23) Wielebinski et al. (1968); (24) Yates et al. (1967); (25) Hill et al. (1958); (26) Bolton & Westfold (1950); (27) Piddington (1951); (28) Ariskin (1981); (29) Landecker & Wielebinski (1970); (30) Hamilton & Haynes (1969); (31) Turtle & Baldwin (1962); (32) Allen & Gum (1950); (33) Dröge & Priester (1956); (34) Ko & Kraus (1957); (35) Wall et al. (1970); (36) Seeger et al. (1965); (37) Pauliny-Toth & Shakeshaft (1962); (38) Haslam et al. (1970); (39) Large et al. (1961); (40) Price (1972); (41) Piddington & Trent (1956); (42) Howell (1970); (43) Moran (1965); (44) Berkhuijsen (1972); (45) Reich (1982); (46) Reich & Reich (1986); (47) Reich et al. (2001); (48) This work.

Table 3: Uncorrected temperatures and spectral index.

Zone	Position	$T_{45}$ K	$T_{408}$ K	$\beta_{45-408}$
Min. South	$l=235^\circ, b=-45^\circ$	3.64E3	1.41E1	2.52
Min. North	$l=192^\circ, b=48^\circ$	3.31E3	1.33E1	2.50
Cal. Point	$l=38^\circ, b=-1^\circ$	3.09E4	1.96E2	2.30
SGP	$b=-90^\circ$	5.58E3	2.04E1	2.55
NGP	$b=90^\circ$	5.16E3	1.92E1	2.54
Anticenter	$l=180^\circ, b=0^\circ$	9.14E3	3.85E1	2.48

- The directions of minimum temperature at 45 MHz in the northern ( $l = 192^\circ, b = 48^\circ$ ) and southern ( $l = 235^\circ, b = -45^\circ$ ) Galactic hemispheres: these directions were selected because the spectral index calculated in these zones is very sensitive to any correction applied to the data.
- The “calibration point” ( $l = 38^\circ, b = -1^\circ$ ): so-called because it was used to calibrate the 45 MHz southern survey (Alvarez et al. 1997b).

Multi-frequency spectral data corresponding to these six positions are given in Table 2. Whenever these values were not in digital format in the literature, they were read directly from the published contour maps. If the publication does not provide an estimate of the errors, we use plus-minus half of the difference between the closest contours.

We applied two extragalactic corrections  $T_{CMB}$  and  $T_{\nu, Ex}$  (see Eq. 2):

- The 2.7 K of the CMB represents different percentages of the sky brightness temperature depending on the position, but especially on the frequency  $\nu$  of the radiation. While at frequencies such as 45 MHz, where the minimum temperature is close to 3500 K, this correction is negligible, it is not at 408 MHz, where the minimum gets close to 13 K.
- The extragalactic non-thermal background. This component is believed to originate from the integrated emission of non-resolved extragalactic radio sources. Appendix A gives a robust estimate of this extragalactic non-thermal spectrum (ENTS, Fig. A.1). We subtract this spectrum from every multifrequency plot, in addition to the 45 and 408 MHz data. This extragalactic emission corresponds to  $\sim 1100$  K at 45 MHz and  $\sim 2.4$  K at 408 MHz.

Figures 3 and 4 show the spectra of the six chosen zones together with least squares (in the log-log scale) fitted lines. Both extragalactic components have been subtracted from the data, and the defined multi-frequency spectral index is the slope of this line. In Table 2, the \* symbol indicates that the point is not included in the least squares fitting. We neglected as an outlier one data value from the calibration point multifrequency fit (Fig. 4, bottom panel). This value, corresponding to 38 MHz (Blythe 1957), lies above the fit by a factor of  $\sim 3$ . We also neglected the data from the minimum south point below 45 MHz, for reasons we detailed below. Neglected data are marked by triangles in Figs. 3 and 4, where the 45 and 408 MHz data are identified by squares. Large discrepancies could be due to real physical features such as thermal absorption at very low frequencies, the steepening of the spectral index towards higher frequencies, instrumental calibration errors, etc ... The points in the minimum-south plot (Fig. 3, bottom panel) below 45

Table 5: Temperature offset corrections in K. Positive values should be subtracted, while negative should be added according to equation (2).

Component	45 MHz	408 MHz
CMB	2.7	2.7
ENTS <sup>a</sup>	1100	2.4
ZLC <sup>b</sup>	-544	-3.46

**Notes.** <sup>(a)</sup> Extragalactic non-thermal spectrum. <sup>(b)</sup> Zero-level correction (see Eq. 2).

MHz were also ignored because we believe they do not represent the real emission of this zone as the large beams associated with these surveys (from  $7^\circ$  to  $15^\circ$  FWHM) wash-out the relatively small area of the minimum-south. Figure 5 illustrates this effect: the contours delineate the minimum south, and the unresolved source just at the side seen in grey-scale is Fornax A, which also represents the 45 MHz antenna beam size. A larger beam would confuse the flux that surrounds the minimum zone (Fornax A flux inclusive) and would infer a higher temperature in this direction. This interpretation is confirmed in Fig. 3 where we can see that the fitted line to the data at frequencies *above* 45 MHz lies below of most of the data points measured at lower frequencies. We tested the spectra of the other five selected areas, and found that removing the low-frequency data does not affect the quality of the fittings significantly. In particular, the minimum-north zone is far more extended than the minimum-south zone, so the antenna beam size does not affect the measured temperature.

In Figs. 3 and 4, we did not include the points at 45 and 408 MHz in the fit because we are trying to find a correction applicable to these surveys based on independent data.

The coordinates of the six zones, the uncorrected temperatures at 45 and 408 MHz, and the spectral index derived from these two values are given in Table 3. In contrast, Table 4 shows temperature and spectral index values corrected by the extragalactic extended components, that is, the ENTS and the CMB. The columns of Table 4 are: “extragalactic-corrected” temperatures, the “extragalactic-corrected” spectral index derived between 45 and 408 MHz, the “extragalactic-corrected” multifrequency spectral index, and the difference between these last two columns ( $\Delta\beta = \beta_{\text{multifreq}}^{\text{extra-corr}} - \beta_{45-408}^{\text{extra-corr}}$ ).

We now explain the quantitative criterion used to evaluate the quality of the fits: having seen that extragalactic-corrected multi-frequency spectra are well fitted by single power laws, as expected if we observe non-thermal synchrotron radiation, we determine zero-level corrections (ZLC) to the 45 and 408 MHz maps such that, when applied uniformly to the six zones, they maximize the sum of the squares of the linear correlation coefficients of the six linear fits.

To summarize, reliable Galactic spectral indices between the 45 and 408 MHz can be derived by applying the ENTS, CMB and the ZLC corrections to both surveys. Table 5 displays all of these corrections. Table 6 shows the 45–408 MHz spectral index corrected values (corrected for ENTS, CMB, and ZLC) and the differences between these corrected temperatures and the multifrequency fit ( $T_{\text{fit}}$ ). These spectral indices and the map derived represent our

Table 4: Extragalactic corrected temperatures and spectral indices.

Zone	$T_{45}$ K	$T_{408}$ K	$\beta_{45-408}^{extra-corr}$	$\beta_{multifreq}^{extra-corr}$	$\Delta\beta$
Min. South	2.51E3	8.98	2.55	2.49	-6.3E-2
Min. North	2.18E3	8.18	2.53	2.41	-12 E-2
Cal. Point	2.98E4	1.91E2	2.29	2.28	-0.9E-2
SGP	4.45E3	1.53E1	2.57	2.57	-0.0E-2
NGP	4.03E3	1.41E1	2.57	2.53	-3.1E-2
Anticenter	8.01E3	3.34E1	2.49	2.48	-0.7E-2

Table 6: Corrected 45-408 MHz spectral indices and differences between the corrected temperatures and the multifrequency fit.

Zone	$\beta_{45-408}^{uncorr.}$	$\beta_{45-408}^{corr.}$	$\frac{T_{45}-T_{fit}}{T_{45}}\%$	$\frac{T_{408}-T_{fit}}{T_{408}}\%$
Min. South	2.52	2.50	-10	-12
Min. North	2.50	2.47	18	10
Cal. Point	2.30	2.29	10	8.5
SGP	2.55	2.53	-6.1	2.1
NGP	2.54	2.52	3.3	5.5
Anticenter	2.48	2.47	12	14

best estimates of the *Galactic* temperature spectral index between these two frequencies.

The isotropic corrections ( $T_{\nu,0} = T_{CMB} + T_{\nu,Ex} + T_{\nu,ZLC}$  in Eq. 2) are

$$T_{45,0} = 550 \text{ K} \quad \text{and} \quad T_{408,0} = 1.6 \text{ K}. \quad (4)$$

Figure 6 shows the final spectral index map.

There are several considerations to take into account concerning the multifrequency spectrum procedure:

- The different resolutions of the data. When comparing different surveys, we really should adopt a common resolution, which we do not here. However, apart from the systematic errors in the measured temperatures at low frequencies in the minimum-south zone, as already explained, the multifrequency spectra show remarkable agreement between independent measures and no significant departure from a single power-law fit. Excluding the minimum-south zone, the zones selected correspond to relatively extended and uniform areas at the resolution of the studies we used. Therefore, differences in beam sizes should not affect significantly the temperature measured in these directions.
- Free-free absorption should produce departures from a single power law, specially at low frequencies that becomes significant at the “calibration point”, which is close to the Galactic plane towards the inner Galaxy. However, the spectrum shown in Fig. 4 (bottom panel) does not show any systematic departure from the straight line fit, at least one that is noticeable beyond the scatter of the points. Therefore, a single power-law seems to be a reasonable fit in each zone.
- Apart from the intrinsic shortcomings of the multifrequency data caused by their low resolution, we believe that these data are very consistent and, in general, we did not find calibration or instrumental errors that question their quality. The determination of spectral indices by means of multifrequency power-law fits should be statistically stronger.

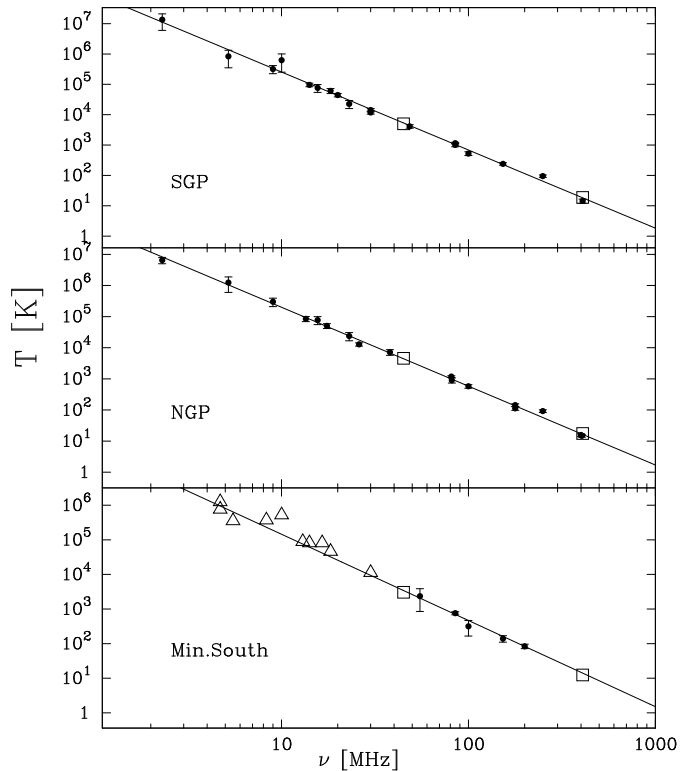


Fig. 3: Multi-frequency spectra of the Galactic component for (from top to bottom): South Galactic Pole, North Galactic Pole, and minimum-south zones. The triangles are not considered in the least squares fitting of the line. The squares represent the 45 and 408 MHz data.

## 4. Discussion of the maps

### 4.1. Scanning and matching effects

The data from low-frequency Galactic surveys are usually obtained by scanning the sky with transit instruments. By “scanning effects”, we refer to the stripes produced in the temperature maps (and particularly noticeable in the spectral index map) because of the different observing conditions, e.g. differences in gain or ionospheric absorption, between adjacent scans made by the instrument. Another spurious effect is produced when surveys made at different epochs or zones or with different instruments are combined in a process described, for example, in Haslam et al. (1981) where the 408 MHz all-sky map was obtained. This effect is caused by the matching of partial maps that together form the final map, and we refer to this as the “matching effect”. All these spurious features and residues are usually produced along constant declination and/or right ascen-

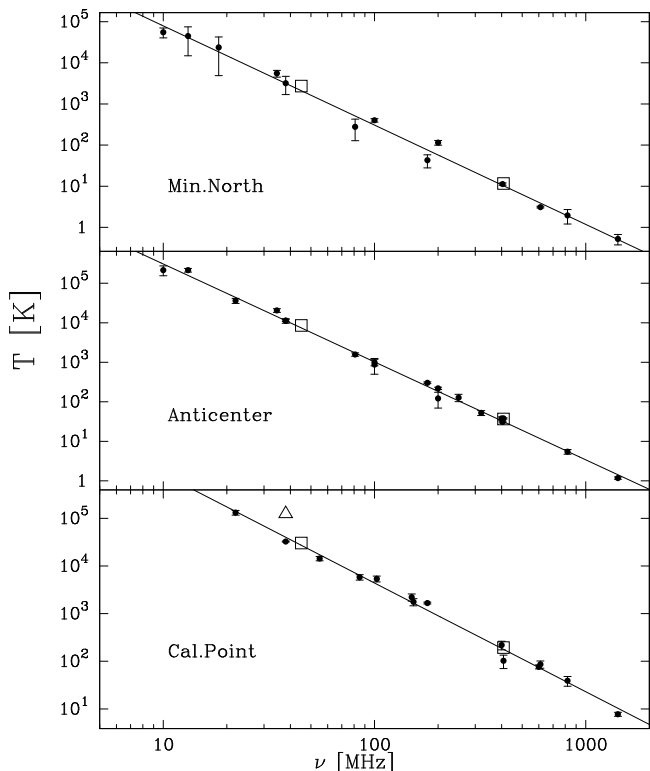


Fig. 4: Multi-frequency spectra of the Galactic component for the (from top to bottom) minimum-north, calibration point and anticenter zones. The triangles are not considered on the least squares fitting of the line. The squares represent the 45 and 408 MHz data.

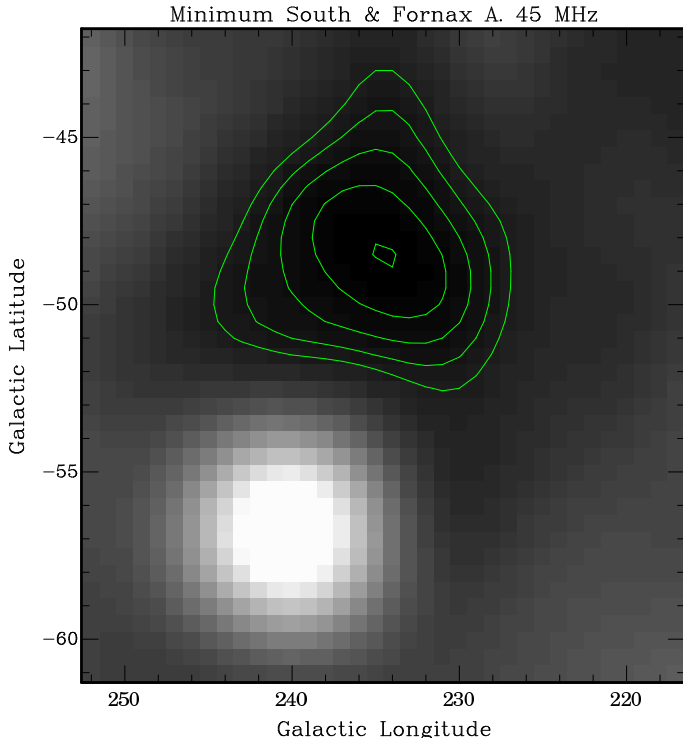


Fig. 5: Minimum-South zone, Plate-Caréé projection and five equi-spaced contours between 3615 and 3870 K. No extragalactic correction applied. The source seen next to the contours is Fornax A.

sion.

The 45 MHz map has a matching effect produced by combining the northern and southern surveys at  $\delta \approx 10^\circ$ . Maeda et al. (1999) calibrated the northern 45 MHz survey using data of the southern survey in a strip of the sky observed with both instruments. The same procedure was used to create the all-sky 45 MHz map presented in this paper. Scanning effects in this survey are present especially at the positions  $RA: 15h \lesssim RA \lesssim 24h$  and  $-30^\circ \lesssim DEC \lesssim 30^\circ$ . They appear at constant declination because both radio telescopes used in the 45 MHz survey were transit instruments. Stripes in the spectral index map at constant RA are due to scanning and matching effects associated with the 408 MHz map, which is formed by combining six different surveys as described in Haslam et al. (1981, Fig 1). Both effects are more important near the zones where the temperature reaches a minimum and are far more noticeable in the spectral index map rather than in the temperature map. The effects described produce some systematic errors in our spectral index at a level lower than 0.05.

#### 4.2. Principal physical processes and characteristics

The principal emission mechanism at 45 MHz is synchrotron radiation from relativistic electrons that permeates the interstellar medium (ISM). The emissivity at a frequency  $\nu$  is proportional to  $H^{\frac{\epsilon+1}{2}} \nu^{\frac{\epsilon-1}{2}}$ , where  $(-\epsilon)$  is the exponent of an assumed power-law distribution of the relativistic electrons energy and  $H$  is the magnitude of the magnetic field. A study of synchrotron emission alone cannot differentiate between the effect of the magnetic field and the characteristics of the fast electron population. Using pulsar rotation measures, Han et al. (2006) placed constraints on the global magnetic field ( $2 \sim 3 \mu\text{G}$  on average in the ISM). Testori et al. (2008) also note from polarization maps of the 21cm continuum that the polarized radio emission is only a few percent (5%) of the total radiation. This may imply that on Galactic scales the “random” component of the magnetic field is far more important than coherent field zones. If this were the case, synchrotron emission would give a direct way of obtaining the relativistic electron column density. If, however, as the three-dimensional Galactic models of Sun et al. (2008) suggest, the regular field is comparable and even more intense than the random field, then the relativistic electron column density can only be obtained from the synchrotron emission with the knowledge of the direction of the regular magnetic field.

The principal absorption mechanism at 45 MHz is thermal absorption from warm ( $\sim 8000$  K) ionized hydrogen. This absorption diminishes the spectral index in the Galactic plane with respect to that at higher latitude. In the multifrequency data, we have seen no obvious absorption feature or departures from a straight-line fit not even in the calibration-point zone (spectral index 2.28), where it would be expected because it is closer to the Galactic plane and in the direction of the inner Galaxy. An absorbed spectra may not differ very much from a non-absorbed one across this range of frequencies. Figure 7 presents two fits to the calibration-point data assuming that the absorption occurs homogeneously along the line of sight. The one displayed with a continuous line assumes that the non-absorbed, purely emission spectrum has an spectral index of

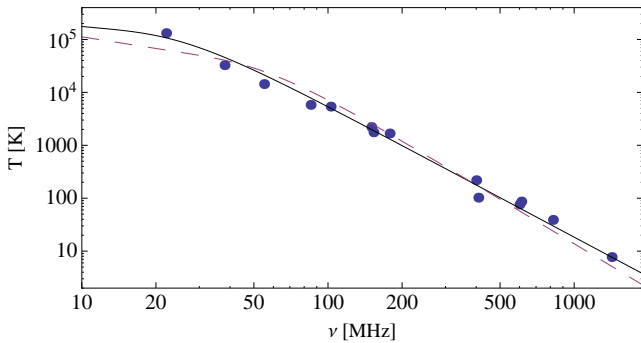


Fig. 7: Fittings to the calibration-point data using a thermally absorbed power-law spectrum with spectral index equal to that at the anticenter (2.48, continuous line) and the value used by Jones & Finlay (1974) (2.80, dashed). Both fittings are reasonable considering the dispersion in the data.

2.48 (the anticenter value), while the other (dashed line), uses a steeper spectrum with spectral index of 2.8. The values derived for  $EM/(\text{cm}^{-6}\text{pc}) \times (T_e/1000\text{K})^{-1.35}$ , where  $EM$  is the emission measure and  $T_e$  is the electron temperature, are 482 and 455, very close to the 470 obtained by Jones & Finlay (1974) towards the  $l = -35^\circ, b = 0^\circ$  direction, which is located in an approximately symmetrical longitude about the Galactic center with respect to the calibration-point ( $l = 38^\circ, b = 1^\circ$ ). Both fittings are fairly reasonable, and the absorption column can take account of the flattening of the spectrum. The emission measures derived assuming  $5000\text{ K} < T_e < 8000\text{ K}$  for the warm ionized gas to produce the absorption seen in the spectral index map are between 1600 and 4000  $\text{pc cm}^{-6}$ , well above the emission measures from the warm ionized medium (Hill et al. 2008). We conclude that this absorption is produced mainly in HII-regions, unresolved by the present survey, implying that the emission measures derived should be regarded as beam-averaged values.

An important characteristic of the map is the presence of two minimum temperature zones, whose multifrequency spectra are shown in Figs. 3 and 4, in the bottom and top panels, respectively. They do not exhibit absorption in the spectral index map discernible by means of a flatter spectrum or a turn-over towards lower frequencies in the multifrequency data. The two zones could be a single volume with either a low density of relativistic electrons or weak magnetic fields. This volume should be nearby judging from its large extension in the sky. There appears to be little correlation with the local bubble described in Lallement et al. (2003), but the positions of the minima are consistent with the super bubble found by Heiles (1998). Interpreting the minimum zones as being produced by a bubble is consistent with both the little absorption detected in their directions and the interpretation of Sun et al. (2008) that high-latitude radio emission comes not from an extended halo-zone but primarily from a local excess of synchrotron emissivity: a local bubble could then explain the minima in these directions. The polarization map of Testori et al. (2008) does not show any conspicuous enhancement or decrement in the polarization fraction toward the southern minimum. We also note that the temperatures measured towards the minima can be considered as upper limits to the extragalactic background.

The maximum spectral index ( $\sim 2.7$ ) is found in a rather flat plateau of approximately  $15^\circ$  diameter around  $l \sim 70^\circ, b \sim +25^\circ$  adjacent to the Northern Spur. This feature is consistent with the results obtained by Webster (1974) (at  $\delta = 40^\circ$ ) and Lawson et al. (1987) who found a steepening of the spectrum in this zone, that is, on the ridge of the Northern Spur rather than on the spur itself. This area of high spectral index is also noted by Roger et al. (1999) between 22 and 408 MHz.

The mean values of the spectral index are consistent with studies made at similar frequencies, for example, Purton (1966) found an spectral index in the halo-high latitude zone of 2.57, close to our mean of 2.54 and Sironi (1974) found a spectral index of 2.53 in the minimum-north between 81.5 and 408 MHz (our value is 2.47). Agreement is better if the zones compared have a relatively constant spectral index because in this case the difference in beam sizes does not affect the spectral index. In contrast, when looking at the anticenter, Purton gets 2.55, a higher value than ours, but within our errors.

The all-sky map compiled by Reich & Reich (1988a) measures spectral indices that are systematically higher by about 0.2 than our map. Webster (1974), who measured the spectral index between 408 and 610 MHz, also obtained values slightly larger than ours. In general, the spectral index appears to increase slightly with frequency in every zone, probably because of aging of the relativistic electron population. The increase in spectral index with frequency on Galactic scales is also obtained by de Oliveira-Costa et al. (2008) through their negative  $\gamma$ -parameter at least at  $\nu \lesssim 1$  GHz, where synchrotron dominates over free-free or the CMB. We do not see a flattening of the spectrum with increasing Galactic latitude at  $l \sim 180^\circ$  as described in Reich & Reich (1988b).

## 5. Conclusions

We have presented a 45 MHz survey that covers more than 95% of the sky and has the advantage of being assembled by data taken with only two radio telescopes of similar characteristics. This map shows the emission from the relativistic electrons being decelerated by the magnetic fields in the interstellar medium. There are two zones of minimum temperature toward  $l \sim 230^\circ$  that are located more or less symmetrically with respect to the Galactic plane. They presumably belong to a single local decrement in the density of relativistic electrons or of the magnetic field magnitude. We have used this map together with the 408 MHz all-sky survey from Haslam et al. (1981) to produce an all-sky spectral index map. We have used a large literature compilation of data to: i) estimate the extragalactic non-thermal emission contribution and ii) implement a method for finding zero-level corrections for radio surveys based on independent data.

The spectral index map has allowed us to derive some conclusions about overall Galactic features: the sky has spectral indices that range between 2.1 and 2.7. Over most of the sky, the index is between 2.5 and 2.6, which is reduced by thermal absorption to values between 2.1 to 2.5 across the Galactic plane strip ( $|b| < 10^\circ$ ). This absorption is probably due to HII regions rather than a more extended global structure such as the WIM. There is a large zone around  $l \sim 70^\circ, b \sim +25^\circ$  adjacent to the Northern Polar Spur where the average spectral index is close to the maximum

of 2.7.

We have also reviewed (Appendix A) estimates of the extragalactic non-thermal contribution in the low frequency range.

## Appendix A: The extragalactic background spectrum

The knowledge of the extragalactic non-thermal spectrum (ENTS), besides its importance on its own, permits a more accurate determination of the emission of our own Galaxy and is another “foreground” component for CMB studies. To separate the radio emission of our own Galaxy from this extragalactic background emission, we have searched the literature to find a reliable estimate of the ENTS. Table A.1 displays the works selected for their *original* estimate of the extragalactic background component. We note that although this is considered an important issue in most radio surveys, only a few authors have made attempts to estimate it:

i) The most common approach is to consider the ENTS as the integrated contribution of extragalactic radio sources, extrapolating their population and distribution from catalogs, and using a cosmological model. Bridle (1967), Simon (1977), Lawson et al. (1987), and Gervasi et al. (2008) used and described the method in detail. In general, the ENTS derived has a spectral index that is about 0.1-0.2 higher than the average emission from our own Galaxy or any other “normal” galaxy. This is attributed probably to the influence of the scarcer but much more luminous radio-galaxies on the ENTS.

ii) Another less common approach is to model the Galactic emission to extract it from the measured data. Yates (1968) and Cane (1979) used simple models consisting of axisymmetric cylindrical components plus arms, spurs, and Galactic sources.

iii) Shain (1959) used 30-Doradus as a thermal absorption screen that at low frequencies blocks the ENTS. Comparison of the emission measured along its line of sight with a nearby one, not-blocked by this HII-region, would cancel out the Galactic component and leave the extragalactic emission.

iv) Baldwin (1967) uses differential spectra to cancel the ENTS and obtain tighter constraints on the Galactic spectrum, which, together with an adequate treatment of the instrumental components, would permit us to obtain the ENTS.

Figure A.1 shows a single power-law fit to the temperatures shown in Table A.1. The best-fit solution is given by

$$\log T = 7.66 - 2.79 \log(\nu/\text{MHz}). \quad (\text{A.1})$$

Whenever the publication was not explicit about the uncertainty in the derived value, we assume it to be twice as large as the errors in the data from where the extragalactic component was derived. From the uncertainty in the data points, we estimate the error in the derived ENTS spectral index to be  $\gtrsim 0.04$ .

*Acknowledgements.* We would like to thank Dr. Patricia Reich for producing the 5° degraded resolution maps at 45 and 408 MHz. J.M. acknowledges partial support from Centro de Astrofísica FONDAP 15010003 and from Center of Excellence in Astrophysics and Associated Technologies (PFB 06).

Table A.1: Extragalactic data obtained from the literature. Lower and upper limits to the ENTS.

$\nu$ MHz	Lower K	Upper K	Ref.
10	4E4	7E4	1
19.7	7E3	2.2E4	2
85	195.	585.	3
100	120	244	4
151	36.3	40.9	5
178	7.5	22.5	6
178	10	13	7
178	19.8	25.8	5
178	23	37	8
610	0.3	0.9	9
610	0.84	0.98	5
1400	0.088	0.102	5
1415	2.95E-2	8.8E-2	9
2700	9.1E-3	1.5E-2	5
5000	3.E-03	3.6E-3	5
8440	3.5E-4	5.6E-4	5

**References.** (1) Cane (1979); (2) Shain (1959); (3) Yates (1968); (4) Clark et al. (1970); (5) Gervasi et al. (2008); (6) Véron (1967); (7) Simon (1977); (8) Bridle (1967); (9) Lawson et al. (1987)

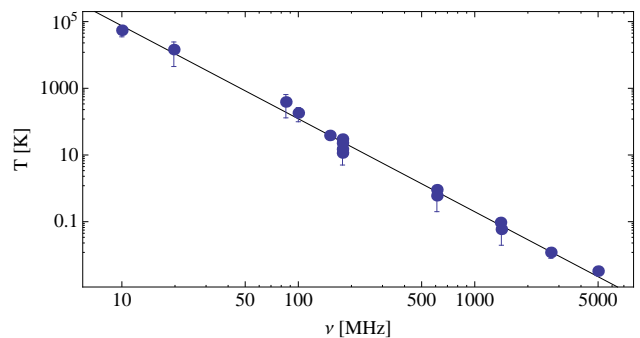


Fig. A.1: Extragalactic component estimates and a single power-law fit.

## References

- Allen, C. W. & Gum, C. S. 1950, Australian Journal of Scientific Research A Physical Sciences, 3, 224  
 Alvarez, H., Aparici, J., & May, J. 1997a, A&A, 327, 569  
 Alvarez, H., Aparici, J., May, J., & Olmos, F. 1994, Experimental Astronomy, 5, 315  
 Alvarez, H., Aparici, J., May, J., & Olmos, F. 1997b, A&AS, 124, 315  
 Andrew, B. H. 1966, MNRAS, 132, 79  
 Andrews, B. H. 1969, MNRAS, 143, 17  
 Ariskin, V. I. 1981, Soviet Astronomy, 25, 558  
 Baldwin, J. E. 1955, MNRAS, 115, 684  
 Baldwin, J. E. 1967, in IAU Symposium, Vol. 31, Radio Astronomy and the Galactic System, ed. H. van Woerden, 337–+  
 Berkhuijsen, E. M. 1972, A&AS, 5, 263  
 Blythe, J. H. 1957, MNRAS, 117, 652  
 Bolton, J. G. & Westfold, K. C. 1950, Australian Journal of Scientific Research A Physical Sciences, 3, 19  
 Bridle, A. H. 1967, MNRAS, 136, 219  
 Cane, H. V. 1979, MNRAS, 189, 465  
 Caswell, J. L. 1976, MNRAS, 177, 601  
 Clark, T. A., Brown, L. W., & Alexander, J. K. 1970, Nature, 228, 847  
 de Oliveira-Costa, A., Tegmark, M., Gaensler, B. M., et al. 2008, MNRAS, 388, 247  
 Dröge, F. & Priester, W. 1956, Zeitschrift für Astrophysik, 40, 236  
 Dwarakanath, K. S. & Udaya Shankar, N. 1990, Journal of



- Astrophysics and Astronomy, 11, 323
- Ellis, G. R. A. 1982, *Australian Journal of Physics*, 35, 91
- Ellis, G. R. A. & Hamilton, P. A. 1966, *ApJ*, 143, 227
- Ellis, G. R. A. & Mendillo, M. 1987, *Australian Journal of Physics*, 40, 705
- Fukao, S., Sato, T., Tsuda, T., Kato, S., & Wakasugi, K. 1985a, *Radio Science*, 20, 1155
- Fukao, S., Tsuda, T., Sato, T., et al. 1985b, *Radio Science*, 20, 1169
- Gervasi, M., Tartari, A., Zannoni, M., Boella, G., & Sironi, G. 2008, *ApJ*, 682, 223
- Hamilton, P. A. & Haynes, R. F. 1968, *Australian Journal of Physics*, 21, 895
- Hamilton, P. A. & Haynes, R. F. 1969, *Australian Journal of Physics*, 22, 839
- Han, J. L., Manchester, R. N., Lyne, A. G., Qiao, G. J., & van Straten, W. 2006, *ApJ*, 642, 868
- Hanbury Brown, R., Davies, R. D., & Hazard, C. 1960, *The Observatory*, 80, 191
- Hartz, T. R. 1964, *Nature*, 203, 173
- Haslam, C. G. T., Klein, U., Salter, C. J., et al. 1981, *A&A*, 100, 209
- Haslam, C. G. T., Quigley, M. J. S., & Salter, C. J. 1970, *MNRAS*, 147, 405
- Haslam, C. G. T., Salter, C. J., Stoffel, H., & Wilson, W. E. 1982, *A&AS*, 47, 1
- Heiles, C. 1998, *ApJ*, 498, 689
- Hill, A. S., Benjamin, R. A., Kowal, G., et al. 2008, *ApJ*, 686, 363
- Hill, E. R., Slee, O. B., & Mills, B. Y. 1958, *Australian Journal of Physics*, 11, 530
- Hornby, J. M. & Williams, P. F. S. 1966, *MNRAS*, 131, 237
- Howell, T. F. 1970, *Astrophys. Lett.*, 6, 45
- Jones, B. B. & Finlay, E. A. 1974, *Australian Journal of Physics*, 27, 687
- Ko, H. C. & Kraus, J. D. 1957, *S&T*, 16, 160
- Lallement, R., Welsh, B. Y., Vergely, J. L., Crifo, F., & Sfeir, D. 2003, *A&A*, 411, 447
- Landecker, T. L. & Wielebinski, R. 1970, *Australian Journal of Physics Astrophysical Supplement*, 16, 1
- Large, M. I., Mathewson, D. S., & Haslam, C. G. T. 1961, *MNRAS*, 123, 123
- Lawson, K. D., Mayer, C. J., Osborne, J. L., & Parkinson, M. L. 1987, *MNRAS*, 225, 307
- Maeda, K., Alvarez, H., Aparici, J., May, J., & Reich, P. 1999, *A&AS*, 140, 145
- Mathewson, D. S., Broten, N. W., & Cole, D. J. 1965, *Australian Journal of Physics*, 18, 665
- May, J., Reyes, F., Aparici, J., et al. 1984, *A&A*, 140, 377
- Milogradov-Turin, J. & Smith, F. G. 1973, *MNRAS*, 161, 269
- Moran, M. 1965, *MNRAS*, 129, 447
- Pauliny-Toth, I. K. & Shakeshaft, J. R. 1962, *MNRAS*, 124, 61
- Piddington, J. H. 1951, *MNRAS*, 111, 45
- Piddington, J. H. & Trent, G. H. 1956, *Australian Journal of Physics*, 9, 481
- Price, R. M. 1972, *AJ*, 77, 845
- Purton, C. R. 1966, *MNRAS*, 133, 463
- Reich, P. & Reich, W. 1986, *A&AS*, 63, 205
- Reich, P. & Reich, W. 1988a, *A&AS*, 74, 7
- Reich, P. & Reich, W. 1988b, *A&A*, 196, 211
- Reich, P., Reich, W., & Testori, J. C. 2004, in *The Magnetized Interstellar Medium*, ed. B. Uyaniker, W. Reich, & R. Wielebinski, 63–68
- Reich, P., Testori, J. C., & Reich, W. 2001, *A&A*, 376, 861
- Reich, W. 1982, *A&AS*, 48, 219
- Roger, R. S., Costain, C. H., Landecker, T. L., & Swerdlyk, C. M. 1999, *A&AS*, 137, 7
- Rohan, P. & Soden, L. B. 1970, *Australian Journal of Physics*, 23, 223
- Seeger, C. L., Westerhout, G., Conway, R. G., & Hoekema, T. 1965, *Bull. Astron. Inst. Netherlands*, 18, 11
- Shain, C. A. 1951, *Australian Journal of Scientific Research A Physical Sciences*, 4, 258
- Shain, C. A. 1959, in *IAU Symposium, Vol. 9, URSI Symp. 1: Paris Symposium on Radio Astronomy*, ed. R. N. Bracewell, 328–
- Shain, C. A. & Higgins, C. S. 1954, *Australian Journal of Physics*, 7, 130
- Simon, A. J. B. 1977, *MNRAS*, 180, 429
- Sironi, G. 1974, *MNRAS*, 166, 345
- Sun, X. H., Reich, W., Waelkens, A., & Enblin, T. A. 2008, *A&A*, 477, 573
- Testori, J. C., Reich, P., & Reich, W. 2008, *A&A*, 484, 733
- Turtle, A. J. & Baldwin, J. E. 1962, *MNRAS*, 124, 459
- Véron, P. 1967, *Annales d’Astrophysique*, 30, 719
- Wall, J. V., Chu, T. Y., & Yen, J. L. 1970, *Australian Journal of Physics*, 23, 45
- Webster, A. S. 1974, *MNRAS*, 166, 355
- Wielebinski, R., Smith, D. H., & Garzón Cárdenas, X. 1968, *Australian Journal of Physics*, 21, 185
- Wolleben, M. 2007, *ApJ*, 664, 349
- Yates, K. W. 1968, *Australian Journal of Physics*, 21, 167
- Yates, K. W. & Wielebinski, R. 1965, *Nature*, 208, 64
- Yates, K. W., Wielebinski, R., & Landecker, T. L. 1967, *Australian Journal of Physics*, 20, 595

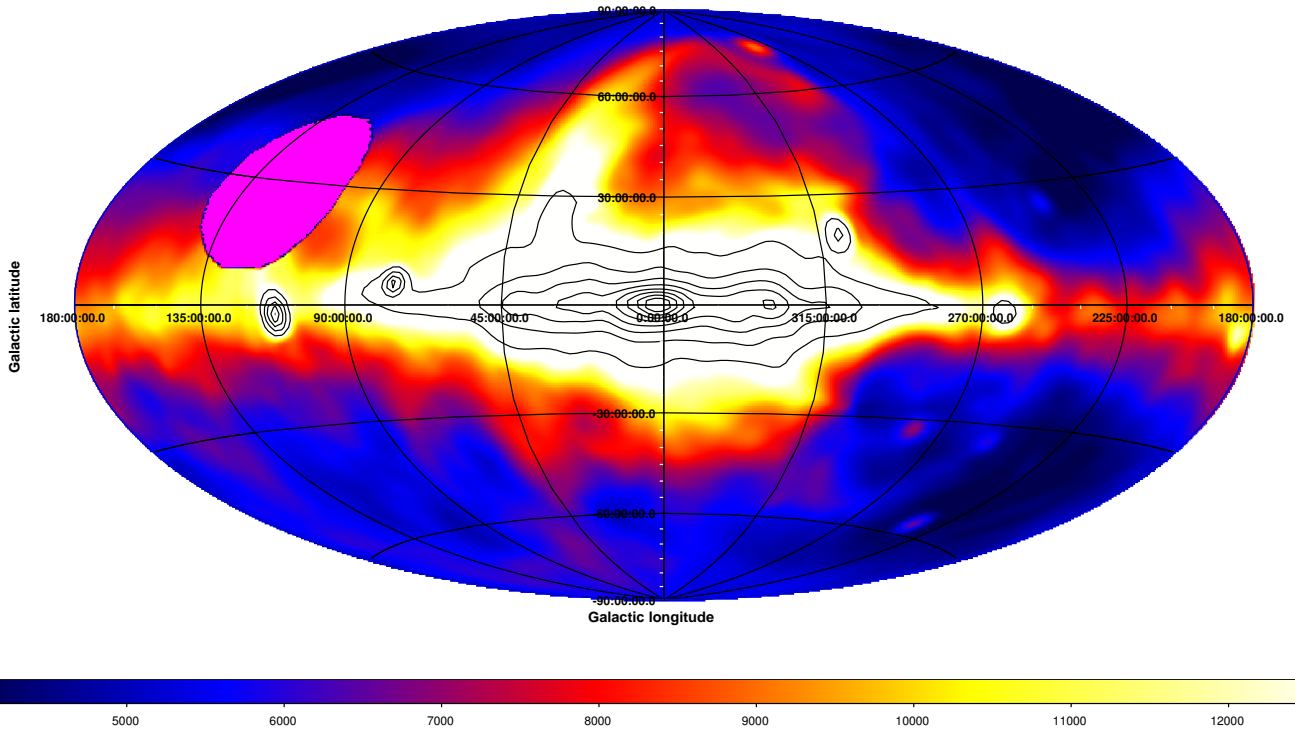


Fig. 1: Hammer-Aitoff projection of the 45 MHz full sky map. Eight contours are drawn between 15000 and 60000 K. The map does not cover the  $\delta > +65^\circ$  zone.

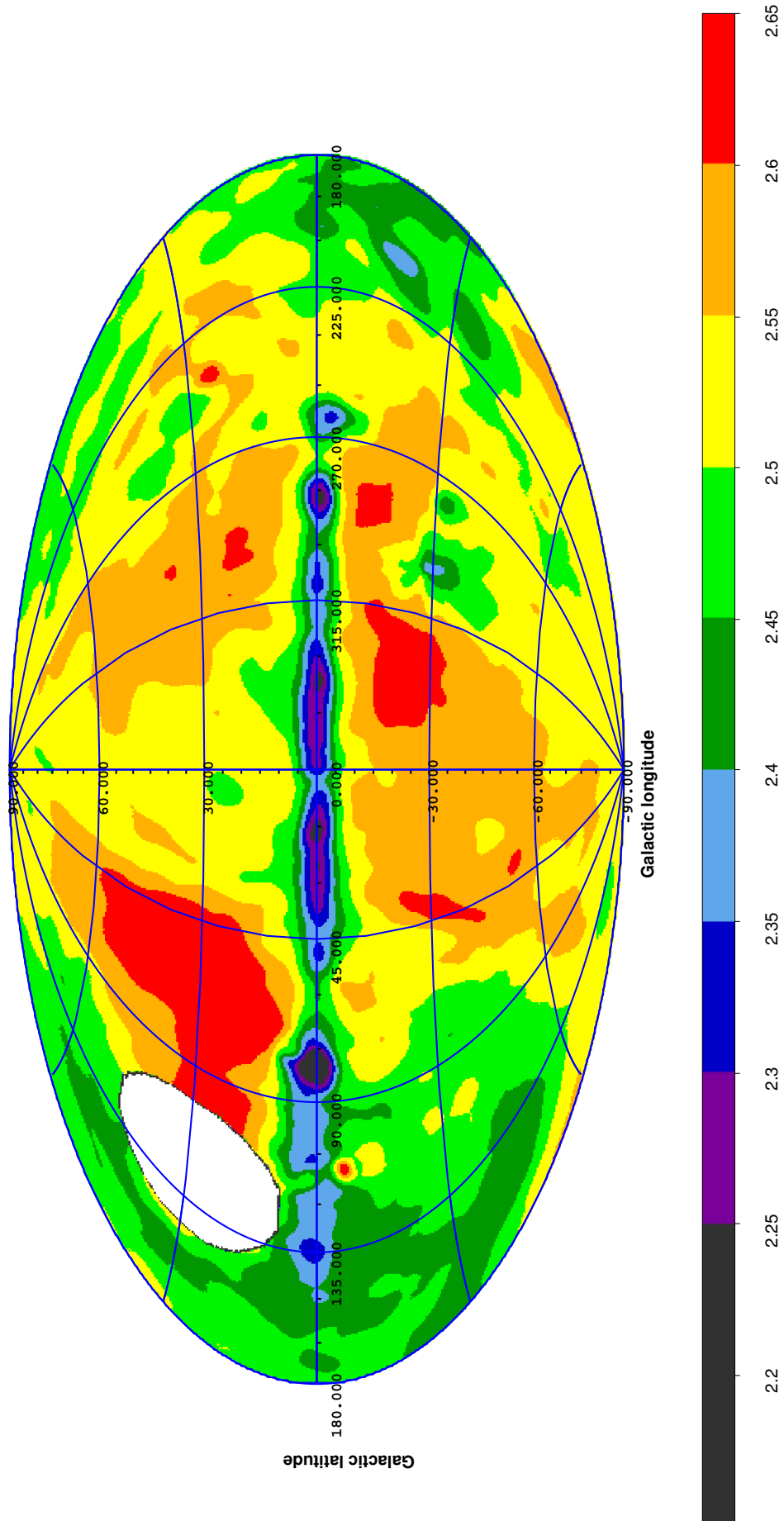


Fig. 6: Galactic temperature spectral index between 45 and 408 MHz with the corrections of Table 6 applied. The map has  $5^\circ \times 5^\circ$  resolution.